International Journal of ENGINE RESEARCH

Standard Article

International J of Engine Research
1–17

DOI: 10.1177/14680874211037118
journals.sagepub.com/home/jer
SAGE

Combustion modelling of turbulent jet ignition in a divided combustion chamber

Mattia Olcuire[1], Clara Iacovano[1], Alessandro d'Adamo[1], Sebastiano Breda[2], Tommaso Lucchini[3] and Stefano Fontanesi[1]

Abstract

Turbulent jet ignition is seen as one of the most promising strategies to achieve stable lean-burn operation in modern spark-ignition engines thanks to its ability to promote rapid combustion. A nearly stoichiometric mixture is ignited in a small-volume pre-chamber, following which multiple hot turbulent jets are discharged in the main chamber to initiate combustion. In the present work, a detailed computational investigation on the turbulent combustion regime of premixed rich propane/air mixture in a quiescent divided chamber vessel is carried out, to study the characteristics of the jet flame without the uncertainties in mixing and turbulent conditions typical of real-engine operations. In particular, the paper investigates the dependency of flame propagation on nozzle diameter (4, 6, 8, 12 and 14 mm) and pre-chamber/main-chamber volume ratio (10% and 20%); CFD results are compared to the experimental outcomes. Results show that the combustion regime in the quiescent pre-chamber follows a well-stirred reaction mode, rendering the limitation in using conventional flamelet combustion models. Furthermore, due to the very high turbulence levels generated by the outflowing reacting jets, also the main chamber combustion develops in a well-stirred reactor type, confirming the need for a kinetics-based approach to combustion modelling. However, the picture is complicated by thickened flamelet conditions possibly being verified for some geometrical variations (nozzle diameter and pre-chamber volume). The results show a general good alignment with the experimental data in terms of both jet phasing and combustion duration, offering a renewed guideline for combustion simulations under quiescent and low Damköhler number conditions.

Keywords

Flame regime analysis, chemistry-based combustion modelling, prechamber combustor, TJI, turbulent jet ignition, RANS simulation, laminar combustion, energy efficient combustion

Date received: 23 February 2021; accepted: 5 July 2021

Introduction

The evergreen purposes to improve engine efficiency and to reduce pollutants formation and fuel consumption are still among the main goals for the automotive industry. Despite the claim for a complete electrification of the passenger car fleet in this decade, CO_2 emissions reduction target, pushed by legislations, can realistically be obtained only by a proper mix of more efficient combustion engines and of hybrid/full-electric powertrains. Problems related to electric energy production, storage and distribution, battery raw materials and lifecycle, recharging time and driving autonomy are still long to be solved, hence the most viable immediate option for a cleaner mobility is hybridization.[1,2] A hybrid vehicle is a complex system where the thermal and electric energy sources are proficiently combined, taking advantage of both. Issues related to electric energy storage and range can be partially overcome thanks to the internal combustion engine (ICE), while tailpipe emissions can be cut down thanks to the development of ad-hoc combustion technologies and strategies. To save costs and weight the thermal unit of a

[1]Dipartimento di Ingegneria "Enzo Ferrari," Università degli Studi di Modena e Reggio Emilia, Modena, Italy
[2]R&D CFD SRL, Modena, Italy
[3]Dipartimento di Energia, Politecnico di Milano, Milano, Italy

Corresponding author:
Mattia Olcuire, Dipartimento di Ingegneria "Enzo Ferrari," Università degli Studi di Modena e Reggio Emilia, Via Vivarelli 10, Modena 41125, Italy.
Email: mattia.olcuire@unimore.it

hybrid vehicle should be as simple and cheap as possible, especially regarding the aftertreatment system, while retaining high performance in terms of fuel efficiency. From a tailpipe emissions standpoint, use of alternative-, e- or CO_2-neutral-fuels combined with ultra-lean combustion seem particularly effective in reducing soot formation[3] CO and NO_x emissions in Spark Ignited (SI) engines.

Cho and Chung[4] highlighted how the NO_x emissions can be strongly reduced by lean hydrogen burn and low-temperature combustion strategies, largely increasing the engine efficiency. The use of lean or ultra-lean mixture can prevent the use of three-way catalytic converters, whose high efficiency is constrained by stoichiometric engine conditions. If combustion temperatures are low enough to avoid NO and N production, which becomes negligible below 1800 K, it could be possible to minimize or even completely remove any NO_x aftertreatment system. Also, under lean conditions cylinder intake pressure needs to be higher, allowing the engine to reduce throttling and therefore pumping losses. Moreover, since SI engines are particularly sensitive to air-fuel ratio (AFR), with air excess combustion can be more complete, reducing the CO production typical of incomplete combustion. Temperature reduction obtained using lean mixtures increases the knock limit[5–7] and, consequently, allows the compression ratio to be raised. Nevertheless, ultra-lean operation gives rise to significant challenges. Quader[8] and Germane et al.[9] highlighted how poor-quality ignition or failure to ignite ultra-lean mixtures can cause misfires and undesired cycle-to-cycle variability,[10] therefore reducing combustion efficiency. Hence, the efficient and reliable combustion of homogenous ultra-lean mixtures remains an ambitious target which requires innovative technologies to increase combustion speed and stability and to overcome potential issues.

To this aim, TJI (Turbulent Jet Ignition) is being given a renewed interest.[11] TJI allows to reach stable combustion of ultra-lean mixtures with high efficiency and low emissions thanks to the adoption of two divided chambers, connected through one or more orifices. TJI uses a small quantity of near-stoichiometric or slightly rich mixture, ignited inside the smallest chamber (usually referred to as 'pre-chamber', PC), which is then forced out by thermal expansion through small orifices into the largest chamber (usually referred to as 'main-chamber' MC). PC combustion induces a pressure gradient between the two chambers, pushing the reacting flow and/or the hot products into the MC. The hot turbulent jets ignite the main chamber lean mixture thanks to the complex coupling of fluid mechanics, thermal effect and chemical kinetics. The radical species inside the jets can result from complete or incomplete combustion, depending on the PC mixture composition and nozzle diameter. They are highly reactive and, containing partially or fully-burnt combustion products, are characterized by very high temperature, allowing the main ignition onset. Furthermore, the high velocity of the jets exiting from the orifices favours the production of turbulent kinetic energy and allows an efficient distribution of reactants in the MC, forming a number of simultaneous highly-reacting hot spots equal to the number of nozzles. Turbulent structures generated by these jets strongly enhance mixing and ignition of the MC mixture; they are deeply influenced by the main chamber temperature because of the mixture viscosity.[12]

The benefit deriving from the adoption of TJI combustion principle has been largely investigated in the last decades. Distaso et al.[13] found a strong reduction of fuel consumption, up to 20%, when using TJI technology. Attard et al.[14] found a 18% improvement in fuel consumption when compared to conventional stoichiometric SI and a strong reduction of NO_x emission due to the near elimination of N_2 dissociation, thanks to the low combustion temperatures. In Attard et al.[15] they found that a PC-initiated combustion allows to reduce the ignition energy demand and therefore the spark plug size, being the ignition driven by the chemical, thermal and turbulent effects of the jets exiting the pre-chamber rather than by the flame kernel growth of conventional SI combustion. They also found very good performance and combustion stability using a single fuel or different fuels for the chambers.[16,17]

The physics behind TJI technology is very complex and hardly attributable to a unique governing aspect, as both turbulence and chemistry have a crucial role in the jet propagation through the nozzles. The ignition process[18] is strongly related to the local mixture and turbulence characteristics which make the PC a difficult system to study through numerical simulations. Ignition is also strongly related to flame quenching, deeply studied by Kyrtatos et al.[19] who classified thermal and hydrodynamic quenching mechanisms. The former occurs when the heat losses towards the nozzle wall exceed the heat release of the flame, whereas the latter is caused by the mixing of the combustion products exiting from the PC with the cold unburnt mixture in the MC.

Several studies investigated the impact of the geometrical details of the combustion chamber(s) on the characteristics of TKI combustion. As mentioned before, nozzle design is also an important parameter for combustion propagation. Being the only link between the chambers, nozzles (both shape and global cross-section) play an important role in jet propagation and PC mixture. Bunce et al.[20] showed that a high number of orifices with low overall cross area results in the highest net thermal efficiency due to the flame front exiting from each of the ignition sites having less chamber volume to cover. Gentz et al.[21] found that jets that are evenly distributed to cover the largest possible MC volume will consume the MC charge more rapidly; faster and more vigorous jets with longer initial penetration are required as the mixture becomes leaner. Biswas et al.[22] investigated the ignition characteristics of a homogeneous mixture inside a pre-chamber combustor,

finding two different ignition mechanisms, namely 'jet ignition' and 'flame ignition'. As the orifice diameter increases, the ignition mechanism tends to switch from jet to flame ignition. The orifice diameter therefore plays a fundamental role in the amount of mass flowing into the PC through the nozzle before the ignition event. It also determines the velocity of the jets entering the MC, and, ultimately, the turbulence promoted by the flame when crossing the nozzle; ultimately, it strongly affects the combustion regime once in the MC. Muller et al.[23] isolated the thermal effect from that of chemical kinetics injecting a mixture of CO_2, H_2O and N_2 into the main chamber. The MC ignition is faster in the reactive species case than in the inert one because of the increase of mean temperature, decrease in ignition delay time and radical proliferation. The authors concluded that the chemical kinetics effects on the turbulent jet are very important and should be considered for TJI simulation and prediction. Moreover, they compared LES and RANS approaches to evaluate the impact of turbulent structures on TJI performance. Strong correlation between vorticity, mixing and temperature were observed. This last aspect is confirmed in which Benekos et al.[12] analysed the effect of unburned mixture temperature, wall temperature and main chamber composition through 2D-DNS studies.

Many studies have already been performed applying TJI to real engines[20,24,25] or rapid compression machines (RCMs) with no uncertainties in terms of fuel/air mixing. In the latter case, an investigation on the performance of the PC combustor varying its geometrical parameters was carried out in Gentz et al.,[21] while Gholamisheeri et al.[26] studied the effect of mixture stoichiometry on jet penetration speed and the same authors[27] discussed the relationship between the reduction of hot jet penetration speed and equivalence ratio, explained in terms of density increases for richer mixtures. Further studies using Rapid Compression and Expansion Machines (RCEMs) were carried out by Bolla et al.,[28] who found that during the jet mixing the mixture in the MC is predominantly ignited by autoignition followed by a progressive transition to a deflagrative premixed flame propagation mode. They also investigated the effects of tangential nozzle angle and volume variation, concluding that the best performance can be obtained with straight nozzles and larger volume, delivering better mixing and faster combustion.[29] Finally, Xu et al.[30] studied RCEM under engine-like conditions, further highlighting the important of initial hot jet speed to drive the MC early combustion.

The combustion regime affecting the flame inside PC, MC and nozzles has not received analogous attention, being strongly correlated not only with the geometrical characteristics of the combustion chamber but also with the local turbulent and chemical scales. In this scenario, CFD simulations can be very attractive to understand the physics behind the observed phenomena. A reliable CFD simulation of combustion can be performed only choosing the most suitable modelling framework for the analysed problem, which in turn is strongly dependent on the combustion regime itself. Under laminar conditions a purely chemical kinetics-based approach is preferable, while a model for turbulence-flame interaction is mandatory when flame propagation is mainly driven by turbulence and flow field (this is the case of the 'flamelet' regime experienced in SI internal combustion engines). In TJI systems it is not possible to a priori decide which choice is to be made, considering that both chemistry and turbulence related phenomena are potentially equally relevant. The study of the combustion regime during PC, orifices and MC combustion can help in understanding what is the best CFD framework to simulate TJI cases in both laboratory test cases and real engine geometries. This is the major aim of the present study. Despite the use of rapid compression machine with homogeneous mixture would allow the investigation of the TJI physics without the uncertainties related to PC mixture composition, very few studies have been conducted with no uncertainties also in terms of turbulence and flow field. For this last reason, in the present study numerical simulations are carried out on a fully premixed and quiescent combustion vessel tested by Yamaguchi et al.[31] The availability of experimental data and the lack of uncertainties in terms of turbulence, mixing and wall temperatures are the reason behind the choice of this test case. Laboratory experiments are simulated using CFD with the aim to understand the reasons behind the experimental evidence. A critical discussion of the combustion regime is carried out to understand what the most suitable modelling framework for this kind of problem is.

Simulated test case and CFD methodology

Experimental conditions

The divided chamber (also named 'bomb') used in the present study is a closed volume combustion vessel described in detail by Yamaguchi et al.[31] and schematized in Figure 1. It consists of a cylindrical MC, with 80 mm of inner diameter and 30 mm of width, and a cylindrical PC, with either 35.7 or 25 mm of inner diameter and same width as the MC. The volume ratio between the tested PC and MC (termed a) is 0.1 or 0.2, which is notably larger than modern type pre-chamber SI engines. The two chambers are connected through a central orifice of 23.7 mm length and different diameters (4, 5, 6, 7, 8, 9, 10, 12 or 14 mm). The divided chamber design and the optically accessible window rendered the study in Yamaguchi et al.[31] a noteworthy example of combustion analysis sharing the same principles and rate-determining factors as modern spark-ignited pre-chamber systems. A single pressure probe is located on the end wall of the MC and a spark ignitor is mounted on the opposite side in the PC. In the simulated cases the divided quiescent chamber is filled by a

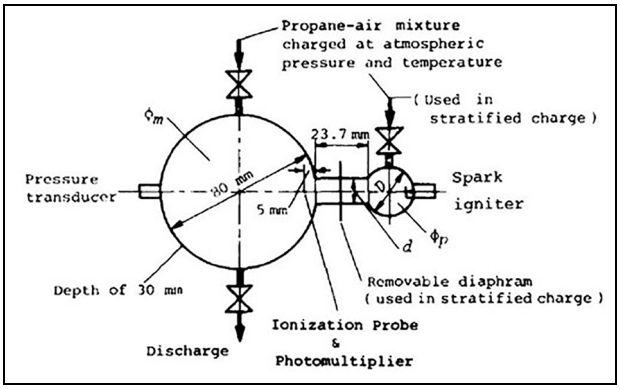

Figure 1. Schematic diagram of the divided chamber bomb from Yamaguchi et al.[31]

rich homogeneous propane-air mixture ($\Phi = 1.1$) at room pressure and temperature (1 bar and 300 K). The most important differences with respect to modern pre-chamber combustion systems are the large PC/MC volume ratio and the quiescent combustion in the PC at ignition; nevertheless, the quality of the combined pressure- and optically-based investigation in Yamaguchi et al.[31] justified the choice of this test case.

From the analysis of the experimental data (Figure 2),[31] a clear connection emerges between the orifice area and the combustion duration, which tends to increase with larger orifice diameters. When using larger nozzles, jet ejection seems to be little affected by the orifice diameter. In addition, a peculiar behaviour of the smallest orifice case is detected: it is in fact the only one showing a very delayed jet exit. Such phenomenon emerges even more evidently when a larger a is adopted. These considerations were made also in Yamaguchi et al.,[31] where ignition was classified into four different types based on the chemical and physical characteristics of the torch jet. The authors justified the more explosive behaviour of the case with the smallest orifice by means of the combined effect of fully dispersed active chemical species and turbulence.

Numerical model

Consistently with the experimental data, a physical duration of 40 ms is simulated. Spark ignition occurs at the beginning of the simulation. Thanks to the two symmetry planes of the real geometry, only a quarter of the domain is modelled to reduce the computational effort. Simulations are carried out using STAR-CD 2020.1, licensed by SIEMENS DISW. A hexahedral computational grid with a base cell size of 1 mm is used. A cylindrical refinement is performed in the PC, the orifice and the portion of the MC exposed to the jet outflow, locally reducing the cell size to 0.5 mm. An analysis of the grid resolution inside the nozzle is performed, pointing out the importance of a double block refinement, reducing the cell size to 0.25 mm. As for near-wall grid, a single layer of 1 mm is adopted, according to the high-Reynolds approach. In the refinement block, the single wall layer reduces to 0.5 mm, while a layer thickness of 0.25 mm is adopted at orifice wall. The total number of cells is approximately 320'000, with minor variations with the orifice diameter or the chamber volume ratio. From a time-step sensitivity analysis, a constant timestep of 8.3×10^{-7} s is used in most of the simulations while the timestep is halved when ignition occurs. The PISO algorithm is used as implicit time integration method, while a second order discretization scheme is used for momentum, turbulence, energy and species.

Coherently with the experimental setup, the flow in both chambers is initially quiescent at room conditions for all cases. The orifice, MC and PC wall temperature is set to 300 K, with a no-slip boundary condition for velocity. A homogeneous air/propane mixture ($\Phi = 1.1$) is initialized in the whole domain. All 3D simulations are carried out within a RANS framework, using the k-ε RNG turbulence model, which is one of the most widely adopted models in the in-cylinder community. The GruMo-UniMORE wall heat transfer model formulation[32–34] is used in all cases.

Due to the quiescent initial state and the ambient conditions, detailed chemical kinetics is incorporated in the model setup for combustion modelling. This approach solves the transport equations for all the species, for which source terms are governed by a detailed reaction mechanism. The C3-mechanism for propane combustion used in the current study is the one proposed by Qin et al.,[35] consisting of 70 species and 463

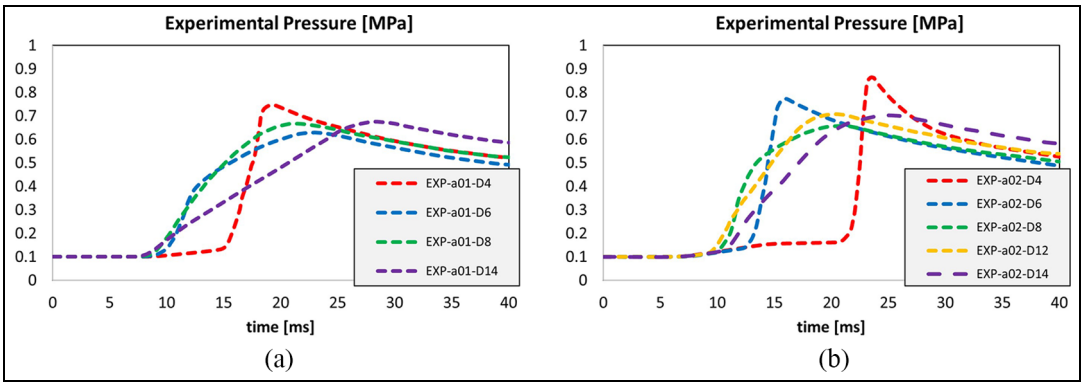

Figure 2. Main chamber pressure trace for a = 10% and 20% in the uniform charge, elaborated from Yamaguchi et al.[31]

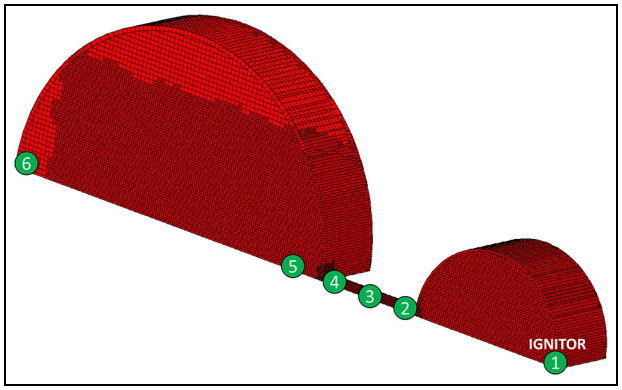

Figure 3. Probes and computational domain, a quarter of the whole geometry is simulated.

reactions. Solving the set of equations is very time consuming so the dynamic multi-zone (DMZ) method is used to create clusters of cells with a similar thermo-chemical state. In the present study, four flow variables are chosen for clustering, that is, temperature (1360 groups), mixture fraction (1000 groups), enthalpy (200 groups) and hydrogen mass fraction (100 groups). As for ignition, this is defined in terms of the spark period, its position, the size of the spark kernel and the ignition temperature. The latter is applied to the reaction rate calculation inside the spark kernel.

Six virtual probes (Figure 3) are used to measure local values of turbulence, pressure, temperature and velocity. Probe1 coincides with the spark electrodes position, while Probe2, Probe3 and Probe4 are used to measure the flow characteristics inside the orifice. Probe5 is set 5 mm downstream from the nozzle exit on the axis, consistently with the ionization probe used in the experiment. Probe6 is in the experimental pressure transducer position.

To compare numerical results with experimental data, the pressure trace is processed similarly to the most common real-engine applications. The sampling covers 40 ms in accordance with the experimental pressure trace acquisition duration. The burnt fraction (X_b) is calculated as in equation (1), which is valid for a constant volume case:

$$X_b = \frac{\frac{\sum_0^{40ms}(V_i * dP_i)}{k-1}}{MAX\left(\frac{\sum_0^{40ms}(V_i * dP_i)}{k-1}\right)} * 100 \quad (1)$$

where k is the specific heat ratio, here considered constant and equal to 1.3 and dP_i is the pressure variation over time.

To further investigate the flame propagation through the nozzle the progress variable (equation (3)) and the chemical reaction zone (equation (4)) are re-calculated.

$$\tilde{c} = \frac{Y_{fuel}}{Y_{fuel\_init}} \quad (2)$$

$$Reaction\ Zone\ Scalar = c * (1 - c) \quad (3)$$

Furthermore, an analysis of the Damköhler number is performed, which is used to weight the contribution of turbulent mixing and of chemical reactions. The Damköhler number Da is calculated as in equation (4), using the length scale $\left(\frac{l_t}{\delta}\right)$ and the velocity scale $\left(\frac{s_l}{u'}\right)$ ratio. The integral length scale l_t and the turbulence intensity u' are calculated as in equations (5) and (6), respectively. The laminar flame thickness δ (equation (7)) is calculated using the Zeldovich correlation.[36,37] λ is the thermal conductivity, ρ_{unb} and $c_{p,unb}$ the density and heat capacity of the fresh gases. s_l is the laminar flame speed, here calculated with a chemistry-based correlation, using a methodology developed in Del Pecchia et al.[38–40] and applied to propane-air mixtures in D'Adamo et al.[41] and equal to approximately 35 cm/s.

$$Da = \frac{\frac{l_t}{u'}}{\frac{\delta}{s_l}} = \frac{l_t}{\delta} \cdot \frac{s_l}{u'} \quad (4)$$

$$l_t = 0.09^{0.75} \cdot \frac{k^{1.5}}{\varepsilon} \quad (5)$$

$$u' = \sqrt{\frac{2}{3}k} \quad (6)$$

$$\delta = \frac{2 * \lambda}{\rho_{unb} \cdot c_{p,unb} \cdot s_l} \quad (7)$$

Results and discussion

Mesh sensitivity

Chemistry-based combustion models usually entail high CPU costs due to the large number of transported chemical species. In the specific case of TJI systems, cost is made even more demanding due to the high velocities reached inside the nozzle, imposing reduced timesteps. To obtain a good representation of the flow field inside the nozzle, it is also crucial to perform a fine spatial discretization. Three cases are performed varying the mesh size in the orifice, set to 0.5, 0.25 and 0.125 mm respectively, as reported in Figure 4. The mesh sensitivity is performed on the geometry with the smallest orifice (4 mm) and the largest volume ratio, named a02-D4 and for which the highest jet velocity is expected. The total number of cells is approximately 286 k (for a cell size of 0.5 mm), 293 k (for the intermediate case) and 333 k (for the finest case).

The numerical pressure trace is computed at the MC probe (n.6), and a high dependence of the orifice flow dynamics on grid density emerges. As depicted in Figure 5, pressure traces are almost superimposed until the flame develops in the PC. Despite all cases correctly show the early pressure rise, only the cases with cell size equal or lower to 0.25 mm well reproduce the subsequent pressure increase, corresponding to MC ignition and combustion. A further comparison between the finer cases is carried out considering wall y^+ (Figure 6) at the maximum velocity time. Low values are found

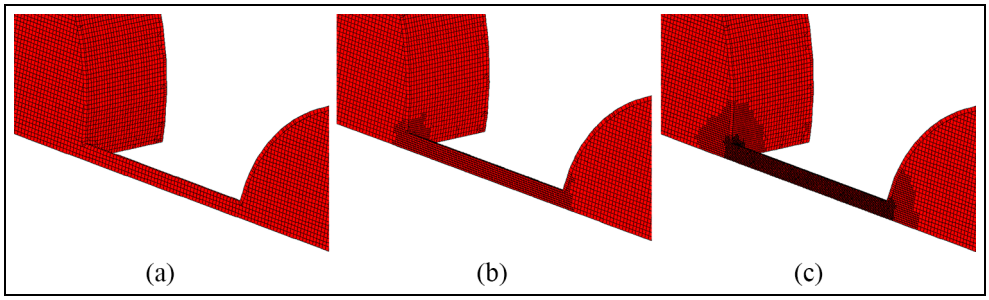

Figure 4. Mesh size inside the nozzle, respectively of 0.5, 0.25 and 0.125 mm.

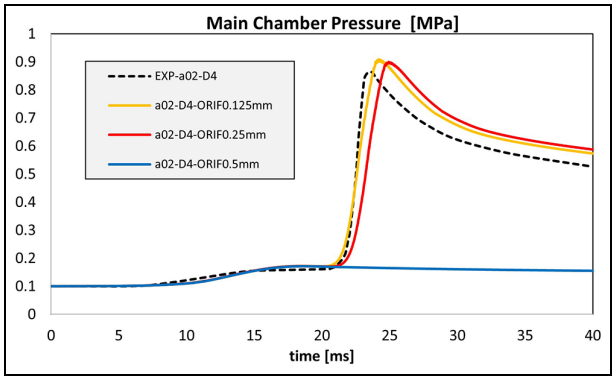

Figure 5. Experimental and numerical pressure traces for $a = 20\%$ and $d = 4$ mm varying the nozzle cell size, measured at main chamber probe.

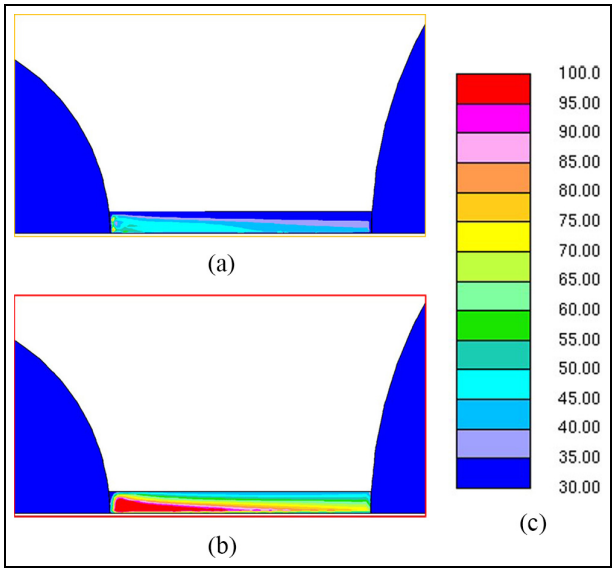

Figure 6. Wall Y^+ when the maximum velocity is reached inside the nozzle, that is, $t = 14$ ms. Cell size of 0.125 mm on the left; 0.25 mm on the right.

over the orifice wall when the finest mesh is adopted. Such grid strategy may lead to potential issues since even lower values are expected when the fluid velocity is lower; this in turn leads to potential errors in the modelling of heat transfer and velocity profiles. Moreover, the 0.125 mm case further increases the computational cost of the simulations because of the highest number of cells and the lowest timestep to comply with the Courant-Friedrichs-Lewy number constraint, especially during the nozzle outflow. As depicted in Figure 7, using a timestep of 8.333×10^{-7} s the average Courant number remains sufficiently low, with maxima equal to 0.22 (during the jet ejection) and 0.28 (when the MC pressure overcomes the PC one, causing a fluid backflow). Therefore, the intermediate orifice cell size of 0.25 mm is chosen in the present study.

Combustion analysis of the smallest orifice diameter and largest PC volume case (a02-D4)

A preliminary analysis is carried out with the highest PC/MC volume ratio and the smallest orifice diameter (a02-D4). Using a kernel radius of 1 mm a satisfactory agreement between experimental and numerical ignition delays is found and the pressure rise phasing is well reproduced (Figure 8). Once the combustion propagates from the PC to the MC it is difficult to determine the nature of the outflowing jet, since a partially quenched flame regime can be expected as a results of

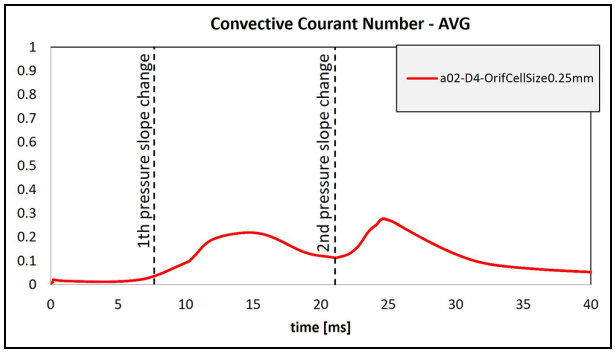

Figure 7. Average Courant number throughout inside the simulation using a timestep of 8.33×10^{-7} s.

intense strain rate and wall interaction during orifice crossing. The experimental pressure trace shows a rapid pressure drop, due to heat exchange, shortly after reaching 90% of fuel burnt, which is well reproduced by the CFD model (Figure 8).

Combustion analysis (Figure 9) confirms a good agreement with the experimental data in terms of both

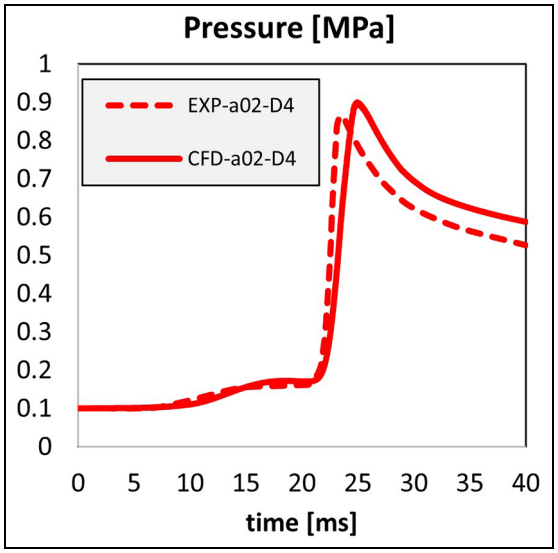

Figure 8. Experimental and numerical pressure traces for $a = 20\%$ and $d = 4$ mm, measured at main chamber probe.

ignition delay and combustion duration, calculated as 0%–10% and 10%–90% of fuel mass fraction burnt, respectively. These are obtained by equation (2), consistently applied to both experiments and simulation results. It is highlighted that the two largest indicators are MFB5 and MFB10 (occurring at 13 and 21 ms, respectively), corresponding to the two slope variations along the pressure trace. This phenomenon affects only this specific case and it will be further investigated hereafter (Figure A1, A2, A3, A4).

The analysis of Mach number in Figure 10 reveals a relatively long phase (approximately 3 ms) in which $Ma > 1$ in the orifice. The related flow chocking concerns the nozzle portion facing the MC, that is, where the highest velocities are reached. In this stage the mass flow rate is physically blocked. This phenomenon is further investigated analysing the local quantities measured by the nozzle probes (Probe3, Probe4 and Probe5), as reported in Figure 11. Partially-burnt and reacting species flow into the MC and diffuse, causing a rapid heat release. Therefore, following a long initial stage of PC combustion, followed by an orifice choking phase, the main portion of combustion is very short.

A deeper analysis of the reaction zone features is performed. A subset of the cells with $0.05 < \tilde{c} < 0.95$

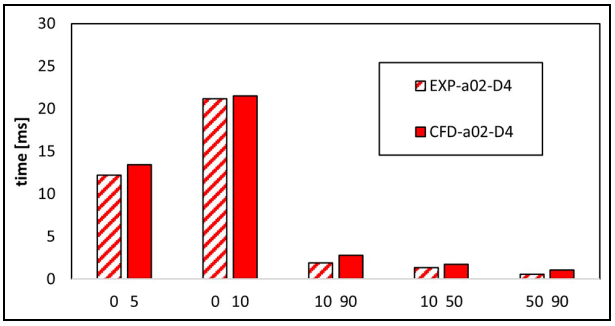

Figure 9. Ignition delay and combustion velocity of $a = 20\%$ and $d = 4$ mm divided chamber bomb.

(equation (3)) is isolated and mass-average quantities on the flame brush are calculated. As shown in Figure 12, due to the ambient quiescent conditions during the early combustion stage, low Da are initially found. Later, a linear-type increase of Da is observed, corresponding to the flame development in the PC. Subsequently the flame experiences the orifice flow, strongly increasing the turbulence encountered by the flame inside the nozzle itself and causing a $Da < 1$ condition shortly before the jet ejection. In the final stage, the reactants diffuse in the MC and a $Da > 1$ regime shift.

The analysis of the Borghi-Peters diagram[42–45] is a fundamental tool to evaluate the flame regime evolution during the combustion process (Figure 13). An investigation of the flame regime is performed via post-processing the length and velocity scales ratio (equation (4)) on the flame brush. This analysis reveals that most of the PC combustion develops in the well-stirred reaction regime ($Da < 1$). During the early flame growth, the reaction kinetics accelerates as temperature increases. This leads to a Da increase, moving the turbulence-chemistry interaction towards a thin reaction zone condition.[46] In the following stage, the flame regime reverts to a well stirred reactor type, due to the high turbulence generated during the jet exit. From here on, the combustion completion lies in proximity of the $Da = 1$ line. Motivated by the above analysis, a chemistry-based combustion model seems to be the most suitable choice when simulating combustion originating from quiescent PC, suggesting that the chemistry rate has a governing role in this case.

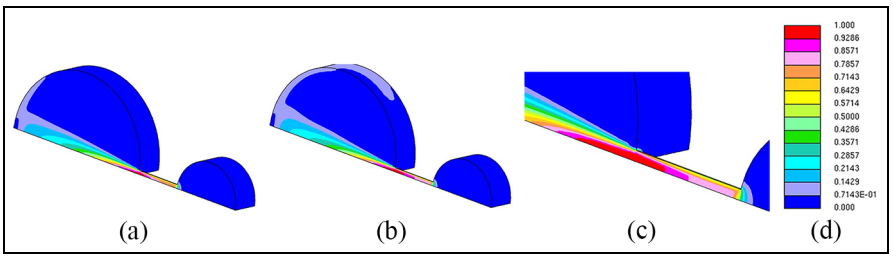

Figure 10. Mach number during chocking onset and end, respectively at 11 and 14 ms. On the right, a detail of the orifice during maximum chocking intensity at 12.5 ms.

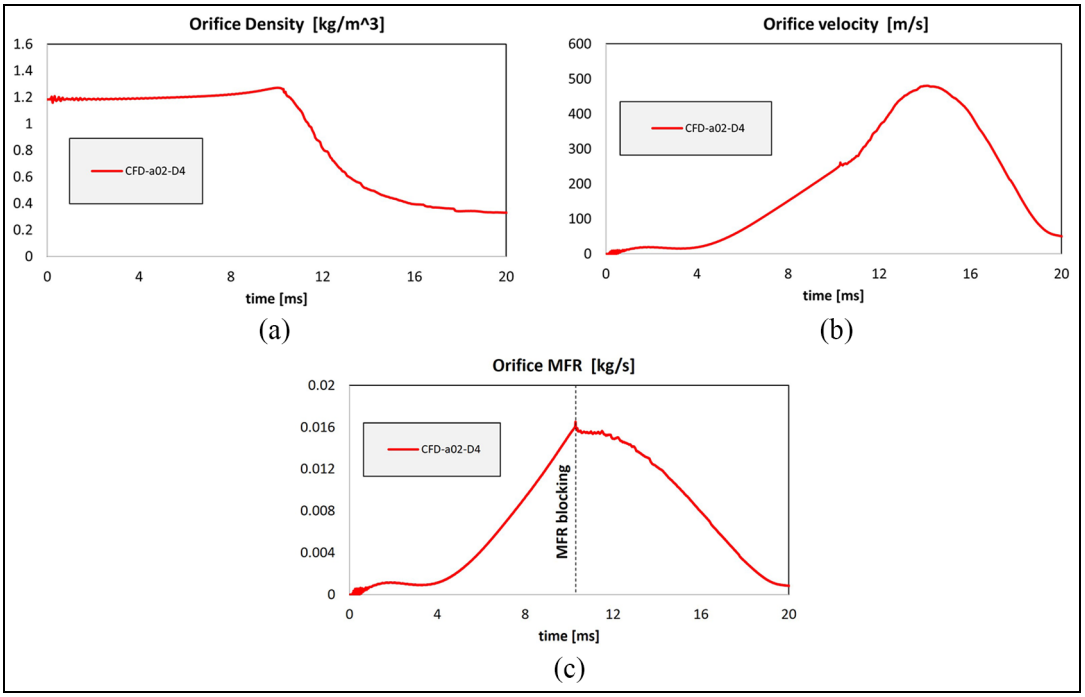

Figure 11. Velocity, density and MFR measured at Probe3 inside the nozzle.

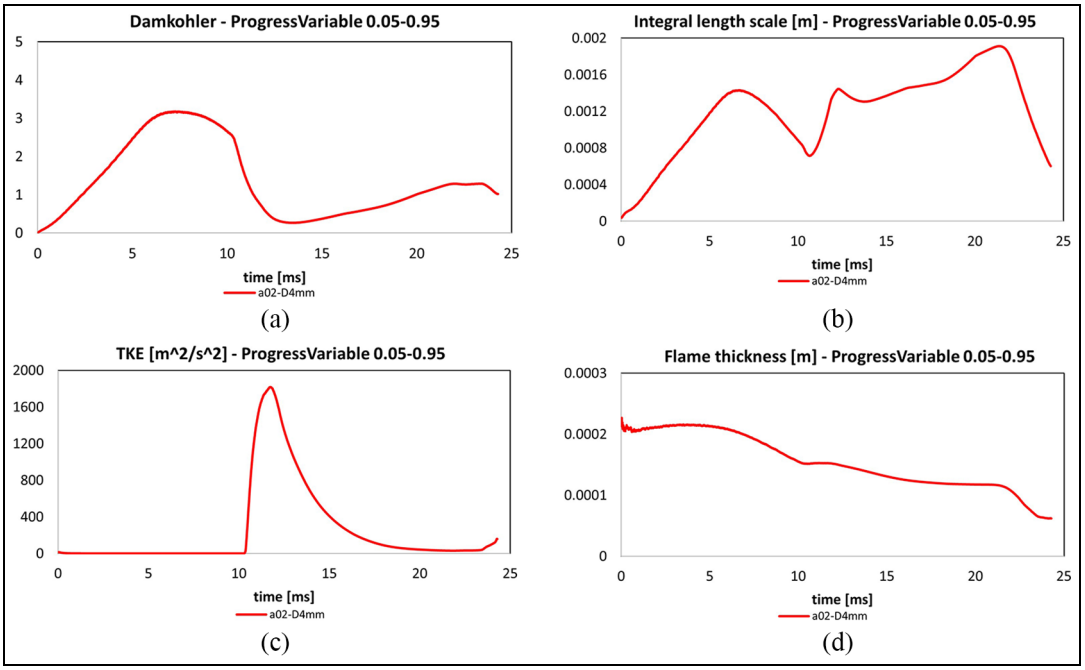

Figure 12. Average quantities seen by the flame, calculated based on the progress variable between 5% and 95%, $a = 20\%$ and $D = 4$ mm.

Orifice diameter analysis

Equal ignition/combustion chemistry-based setup was applied increasing the orifice diameter until 14 mm, on equal PC/MC volume ratio, that is, 20%. As mentioned, in the experimental data the two slope changes are observed only for the D4 case, and the jet exit phasing is generally advanced compared to the previously analysed case, indicating the absence of flow choking. Furthermore, faster combustion development is observed for the narrower nozzle cases. As depicted in Figure 14, from the analysis of the pressure traces it is notable that the anticipated jet ejection from the smallest orifices is well predicted also by 3D model. Once the orifice diameter is large enough to avoid choking, the jet exit seems to be less affected by the nozzle area variation: all the cases with $D \geqslant 6\ mm$ show only one

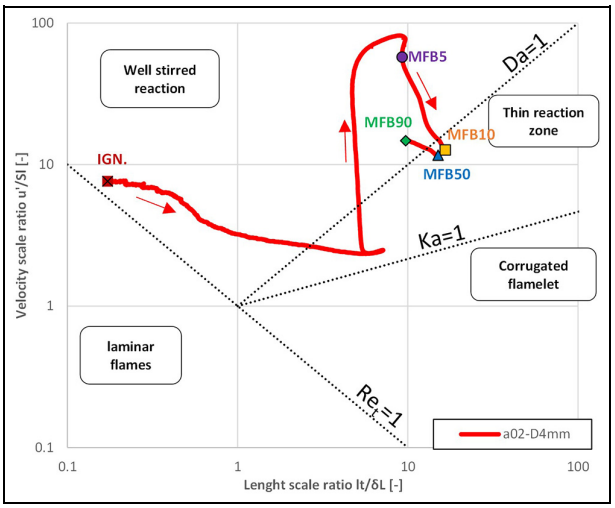

Figure 13. The combustion outcome of the a02-D4 case is presented in the Borghi-Peters diagram.

slope change of the pressure trace and all of them are similarly phased. On the contrary, 10%–90% burn duration is largely dependent on the orifice section.

From the burnt fraction analysis reported in Figures 15 and 16, several considerations can be made on the sensitivity to the orifice diameter. The time delay between 5% and 10% of fuel burnt is very short for all other cases (except for the nozzle-choked a02-D4 case), and both 5% and 10% duration indicators are quantitatively aligned with experimental data. The late-combustion indicators (10%–50% and 10%–90%) increase for larger orifice diameter, again in agreement with the experiments. It is to be noted that the predictive capability of the model is not optimal for large D cases.

A comparison of the flame shape at MFB10 is shown in Figures 17 and 18. A strong correlation between the jet front structure and the orifice area is notable: as the orifice diameter decreases, the flame reaches higher velocities inside the nozzle, resulting in longer penetrating jets. Also, the spread of chemical species which characterizes the smallest orifice, promoted by the long choked-flow phase, is not visible in the larger nozzle cases on equal burn duration. The $D = 4\,mm$ case is both the smallest orifice one and the only choked case, resulting in the lowest mass flow rate and the wider dispersion of reactive species in the MC.

The analysis of the probes located inside the domain shows that a $D \geqslant 6\,mm$ orifice is sufficient to considerably reduce the pressure unbalance between PC and MC (Figure 19), approaching null values for $D \geqslant 8\ mm$ orifices. Consequently, the flow velocity through the nozzle drops significantly with larger nozzles.

The quantities evaluated in the $0.05 < \tilde{c} < 0.95$ range are analysed for all the cases and reported in Figures 20 and 21. The Damköhler numbers seen by the flame inside the PC are little affected by the increasing orifice area. As for the turbulent kinetic energy encountered by the flame in the $D = 4 - 6\ mm$ cases, values one order of magnitude higher than those with the largest nozzles are measured. Due to the very fast combustion of the D4 case, an almost constant average Da is found during its main chamber combustion. On the contrary, Da increases during combustion progress for D6–14 cases. These considerations apply also to combustion regime analysis (Figure 22), further confirming the reduced dependency on the orifice diameter on the PC flame regime. The lower turbulent kinetic energy found for large D cases moves the MFB50 and MFB90 towards the thin reaction zone: this could motivate the burn duration misalignment with experimental data for these cases. However, most of the combustion process develops in the well-stirred reaction zone, pointing out the importance of using a chemistry-based combustion model.

PC/MC volume ratio analysis

A deeper investigation of the effect of the geometrical characteristics of the PC on the flame regime is

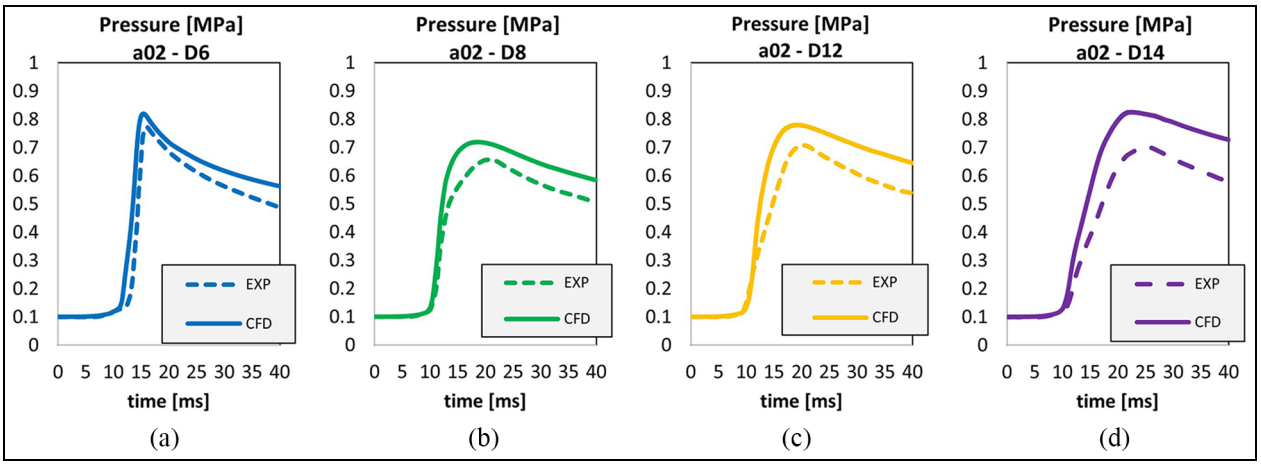

Figure 14. Experimental and numerical pressure traces for $a = 20\%$, measured at main chamber probe.

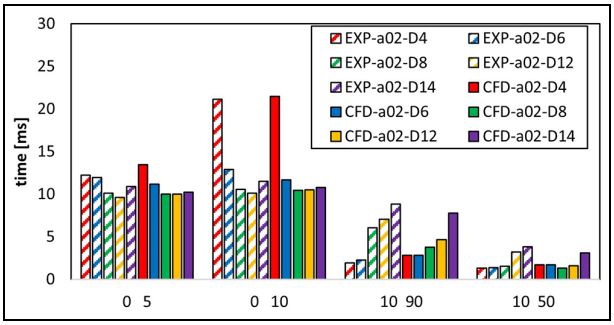

Figure 15. Ignition delay and combustion velocity for different orifice diameters, $a = 20\%$.

performed. The same ignition/combustion setup is applied for the cases with the lower PC/MC volume ratio, that is, 10% (Figure 23). The analysis of the experimental data shows an earlier jet ejection, as well as a slower combustion. Also in these cases the D4 configuration (a01-D4) is the only outlier, with a notably delayed jet ejection compared to the larger nozzles.

The numerical pressure traces show that from a qualitatively standpoint the sensitivity on the orifice area is well reproduced by CFD simulations. The delayed jet exit of the a01-D4 case is appreciable, even if a slight underestimation is observed. In this case $Ma < 0.8$, but the delayed jet ejection is motivated by the obstruction

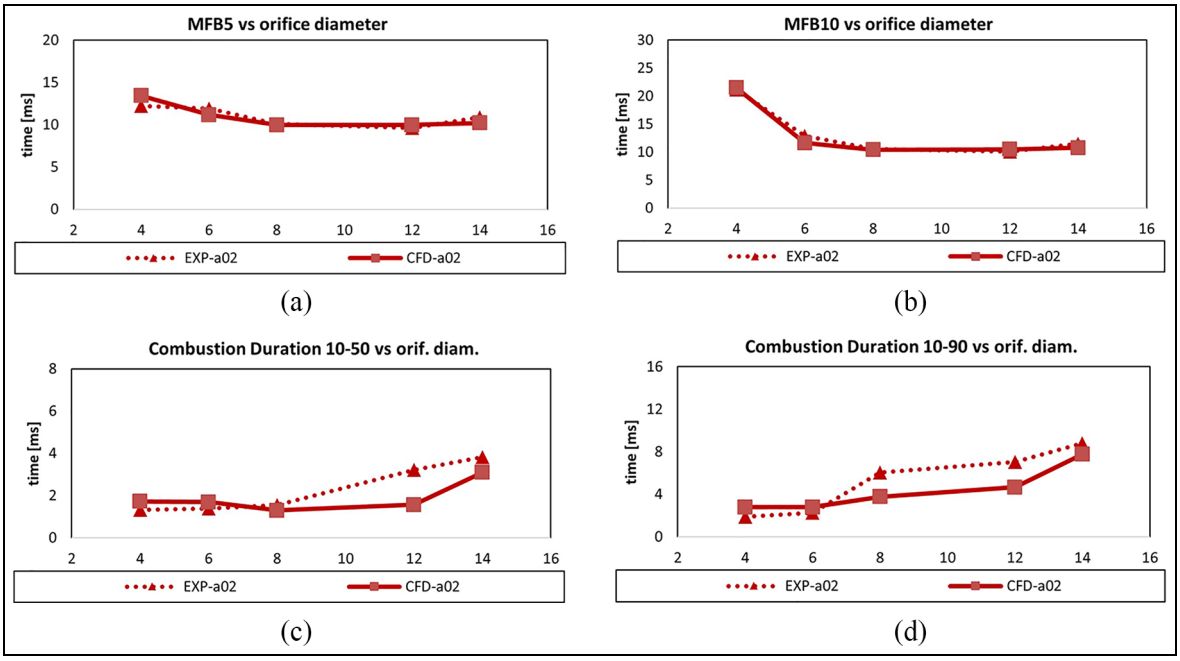

Figure 16. Ignition delay and combustion orifice varying the orifice diameter, $a = 20\%$.

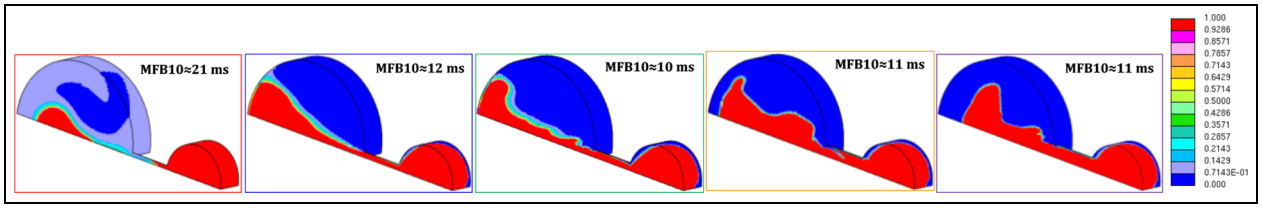

Figure 17. Progress variable at MFB10 for orifice diameters of 4, 6, 8, 12 and 14 mm.

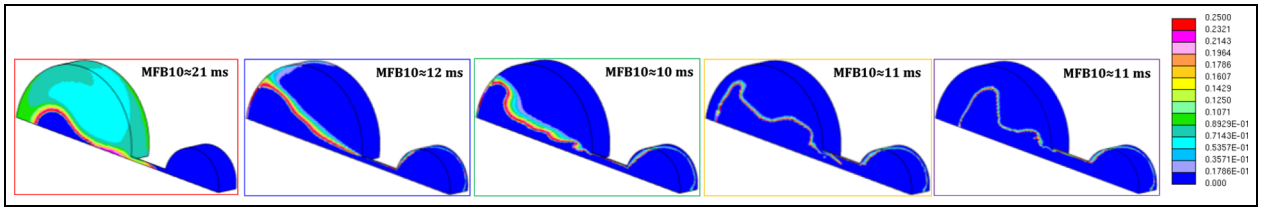

Figure 18. Reaction front at MFB10 for orifice diameters of 4, 6, 8, 12 and 14 mm.

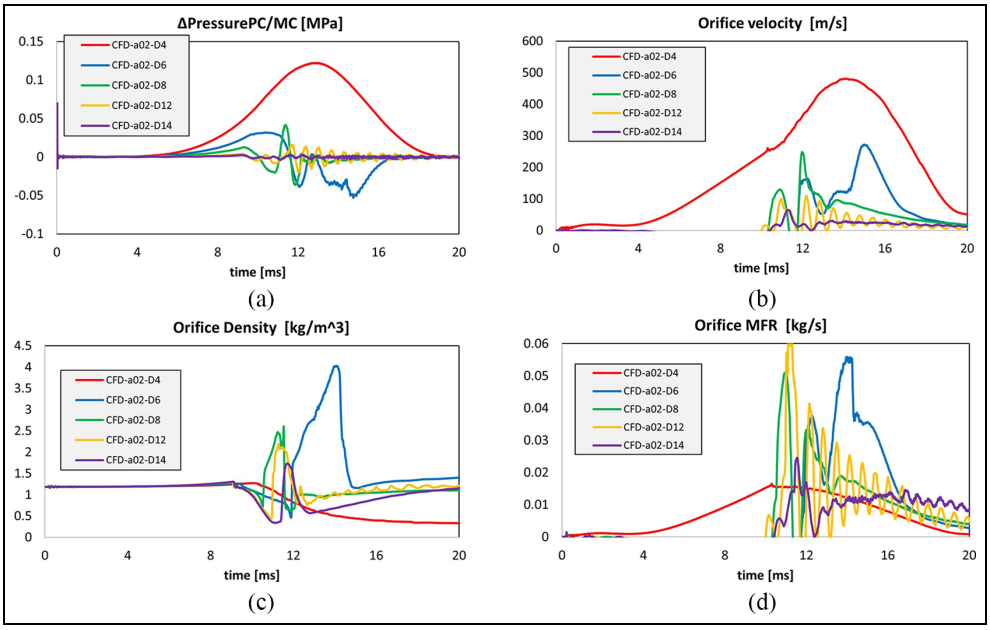

Figure 19. ΔP between the chambers. Axial velocity, orifice density and MFR through the nozzle, $a = 20\%$.

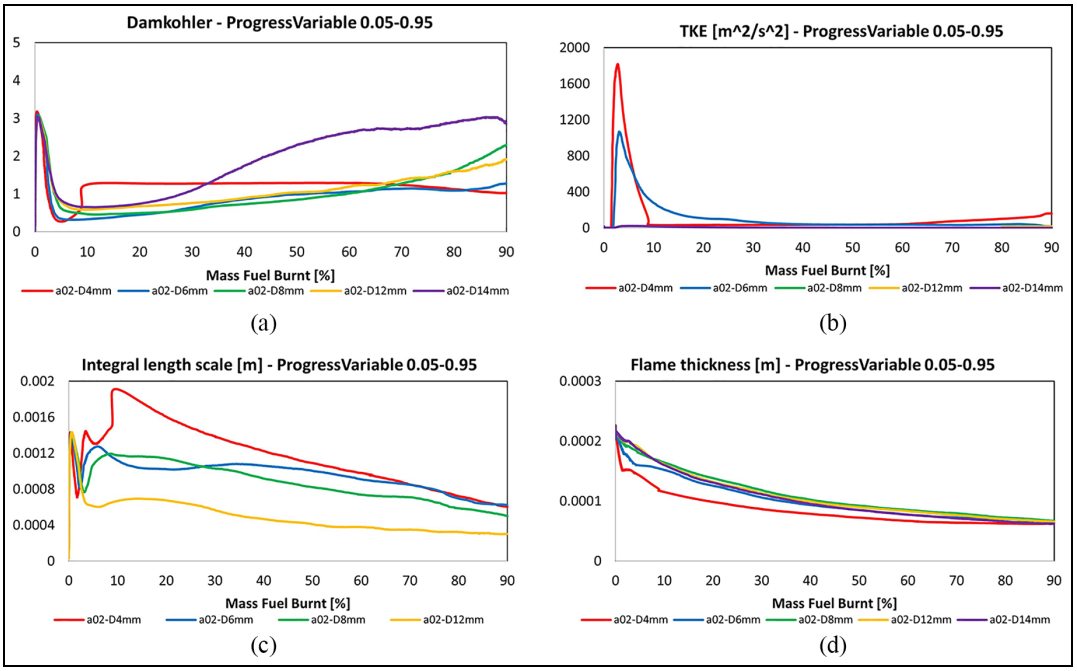

Figure 20. Average quantities seen by the flame, calculated based on the progress variable between 5% and 95%, $a = 20\%$.

of the small-area orifice. A further confirmation comes from the analysis of HRR in Figure 24: both 5% and 10% combustion indicators are very close even for the D4 case, excluding any evidence of chocking conditions. Comparing the numerical results with the experiments in terms of 5% and 10% phasing, a good agreement is found and the experimental trend is well reproduced by CFD simulations. From a quantitative standpoint, 10%–50% burn duration well matches the experimental reference for all cases except a01-D14.

The analysis of the combustion regime throughout the simulation duration (Figures 25 and 26) reveals that the combustion in the PC is still dominated by a well-stirred reaction condition, further motivating the need for a kinetic-driven modelling framework. A small PC volume leads to lower $\Delta p_{PC\text{-}MC}$, in turn promoting low turbulent kinetic energy values inside the nozzle. The *Da* values in the MC for the $a = 10\%$ are generally higher than those for $a = 20\%$, and the combustion regime early moves into the thin reaction zone. Unlike

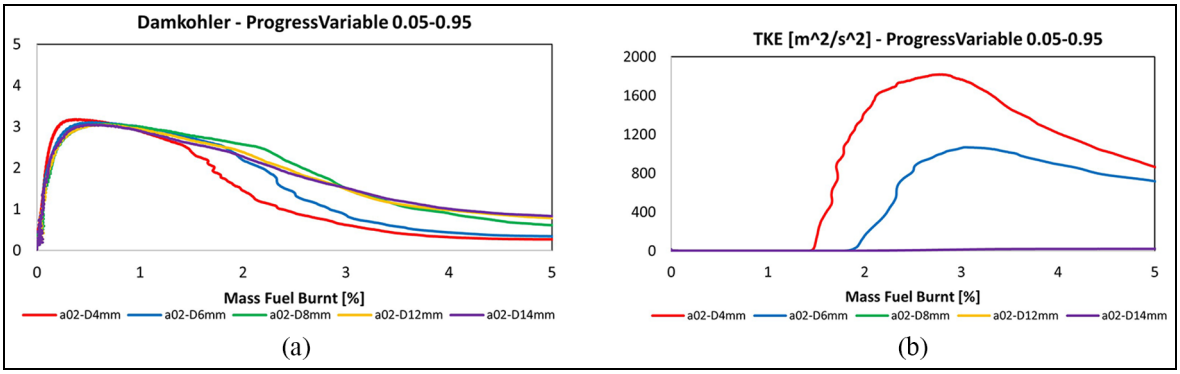

Figure 21. Average quantities seen by the flame until the jet ejection, calculated based on the progress variable between 5% and 95%, $a = 20\%$.

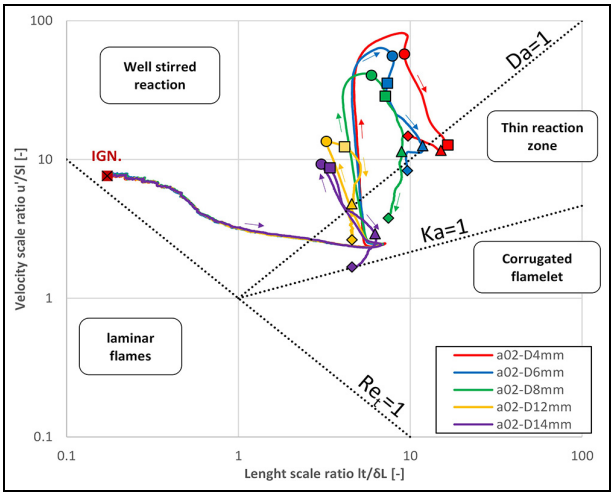

Figure 22. The combustion outcome of all test conditions involving $a = 20\%$ are presented in the Borghi-Peters diagram. Circles correspond to MFB5, squares to MFB10, triangles to MFB50 and rhombus to MFB90.

cases with $a = 20\%$, the combustion phasing (MFB50) of each case now falls into the thin reaction zone. Noticeably, the end of combustion (e.g. MFB90) of the larger-D cases moves in the corrugated flamelet regime, pointing the possibly out-of-range condition of the adopted kinetics-driven approach in this case as the reason for the combustion velocity underestimation for the a01-D14 case.

Figure 27 summarizes the comparison of all the simulated cases (a01/02, D4/14) with the experimental counterparts. Noticeably, a very good alignment is found for MFB5 and MFB10 indicators, driven by PC combustion. The agreement of combustion velocity is appreciable also in the MC combustion phase with no model tuning, especially for the a02 and low-D cases. Only the a01-D14 case shows a slower combustion compared to the experimental data, for the reasons discussed above.

Conclusions

A detailed numerical investigation on the flame combustion regime of premixed propane/air mixture in a quiescent divided chamber bomb under ambient conditions is carried out. The availability of experimental data, the absence of mixing uncertainties and flow field inside the chambers make this test case suitable for a solid preliminary study. Due to the quiescent initial

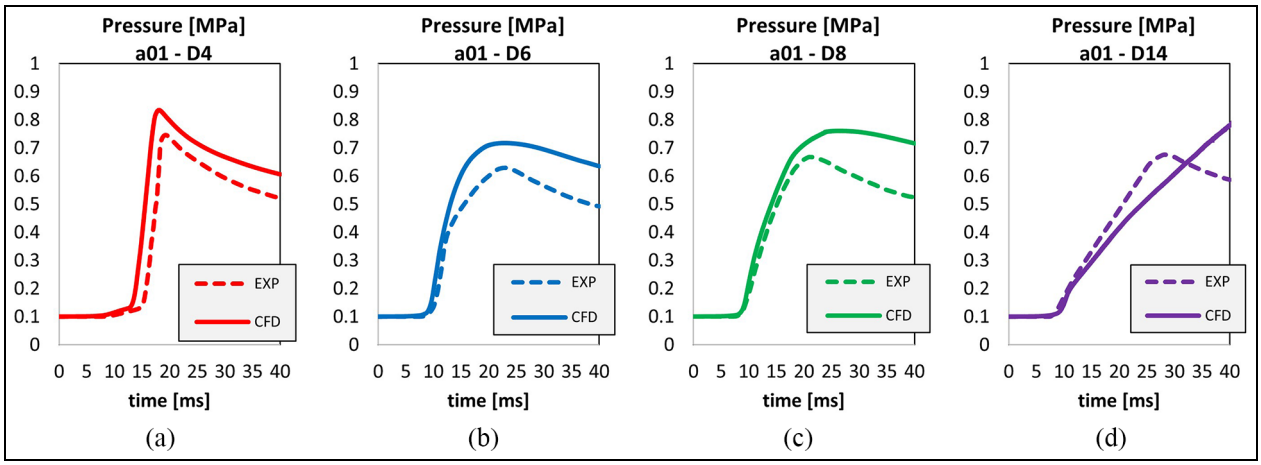

Figure 23. Experimental and numerical pressure traces for $a = 10\%$, measured at main chamber probe.

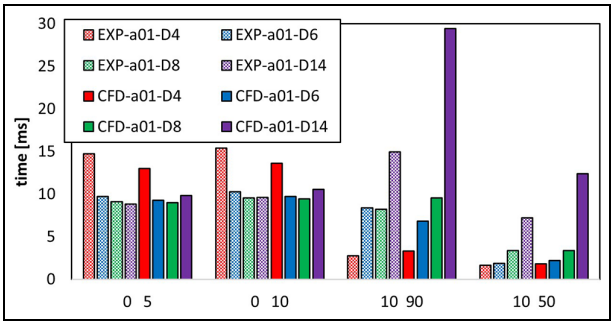

Figure 24. Ignition delay and combustion velocity for different orifice diameters, $a = 10\%$.

state and the low temperatures affecting this case, detailed chemical kinetics is incorporated in the model setup and a kinetics-driven combustion modelling framework is adopted for the present study. A single ignition and combustion setup is shared by all the cases, to avoid tedious case-by-case tuning of the modelling framework. A very good agreement is found with the experimental jet phasing both varying the nozzle diameter and the chamber volume ratio. First, a preliminary 3D analysis is carried out using the orifice diameter of 4 mm, leading to the following consideration: combined small nozzle diameter and higher volume ratio induce a long chocking phase inside the orifice, which in turn causes the combustion in the main chamber to be more explosive, due to the simultaneous effect of turbulent hot jet and fully dispersed active species. Combustion duration of the largest pre-chamber is found to be well aligned with the experimental data varying the orifice diameter. Decreasing reliability of the model is found for larger nozzles. This may be explained considering the flame regime which affects such case: due to the much lower turbulence resulting from the decrease of the pre-chamber volume and the increase of the orifice diameter, the Damköhler number seen by the flame tends to move the flame regime outside the well-stirred reaction zone, highlighting limitations of the kinetic-driven approach when moving into the thin reaction zone. The combustion duration of the smallest pre-chamber well matches the experiments for the smaller orifices, but it tends to be underestimated when increasing the nozzle diameter up to 14 mm. However, due to the very low turbulent kinetic energy encountered by the flame inside this nozzle, the main chamber flame regime falls into the corrugated flamelet zone, highlighting the limitations of a purely kinetics-driven modelling framework.

The presented study shows a fundamental investigation aimed at understanding the flame behaviour and its own regime using a pre-chamber combustor, without the uncertainties which may affect real-engine cases or RCEM applications. Further studies must be performed to investigate the use of more traditional flamelet combustion models, as well the use of kinetic-driven approaches under actual engine-like conditions. The conducted analysis also suggests the need to develop hybrid flamelet/kinetic models, whose adoption seems crucial in pre-chamber combustion systems where a priori assumptions on specific combustion regimes are very likely to fail. In this context, combustion models

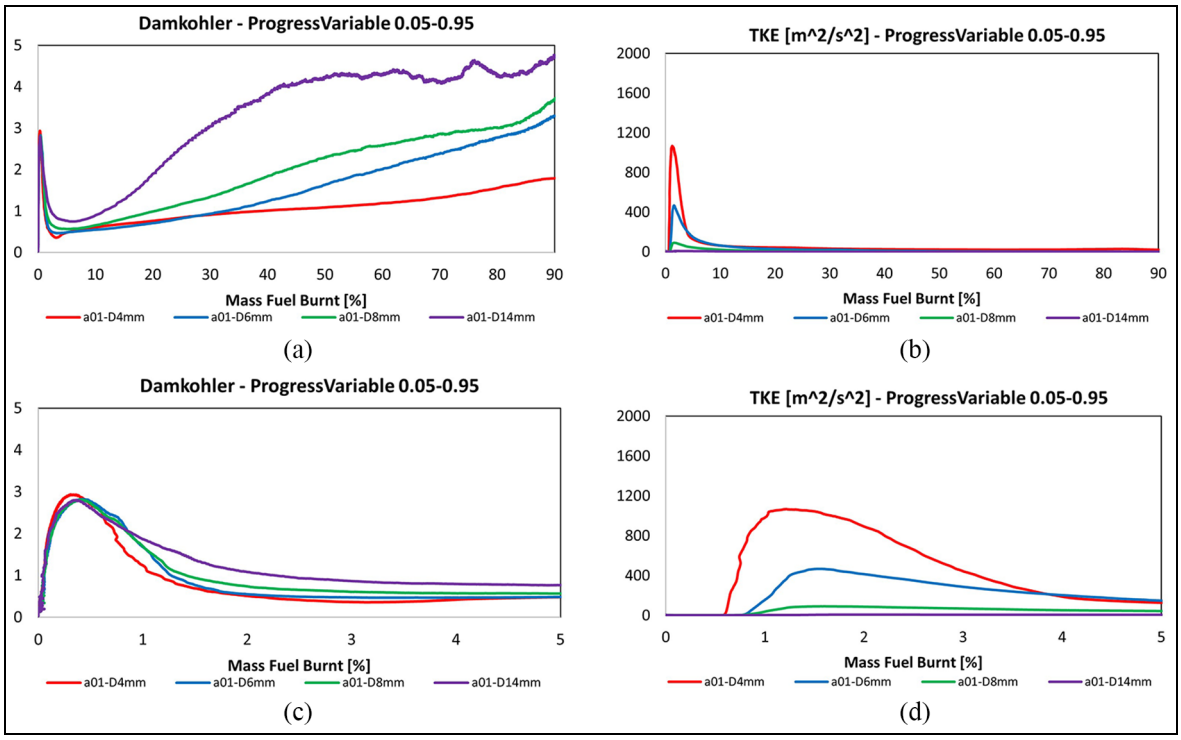

Figure 25. Average quantities seen by the flame, calculated based on the progress variable between 5% and 95%, $a = 10\%$.

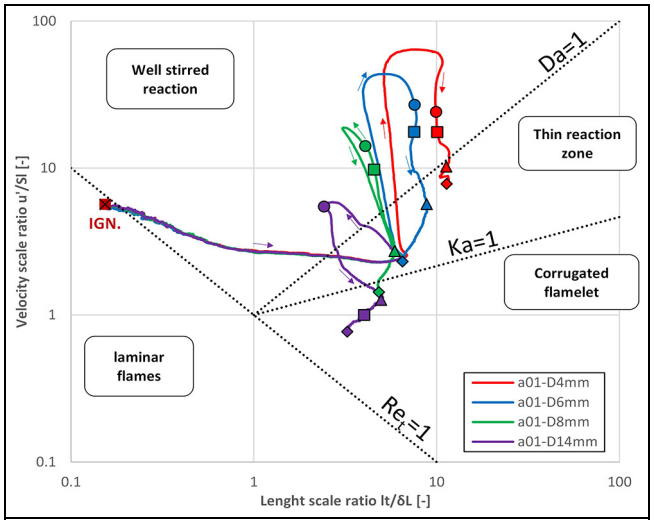

Figure 26. The combustion outcome of all test conditions involving $a = 10\%$ are presented in the Borghi-Peters diagram. Circles correspond to MFB5, squares to MFB10, triangles to MFB50 and rhombus to MFB90. Most of the combustion inside the pre-chamber falls into the well-stirred reaction zone. Increasing the orifice area, the main chamber combustion regime tends to move into the thin reaction zone and even into the corrugated flamelet zone.

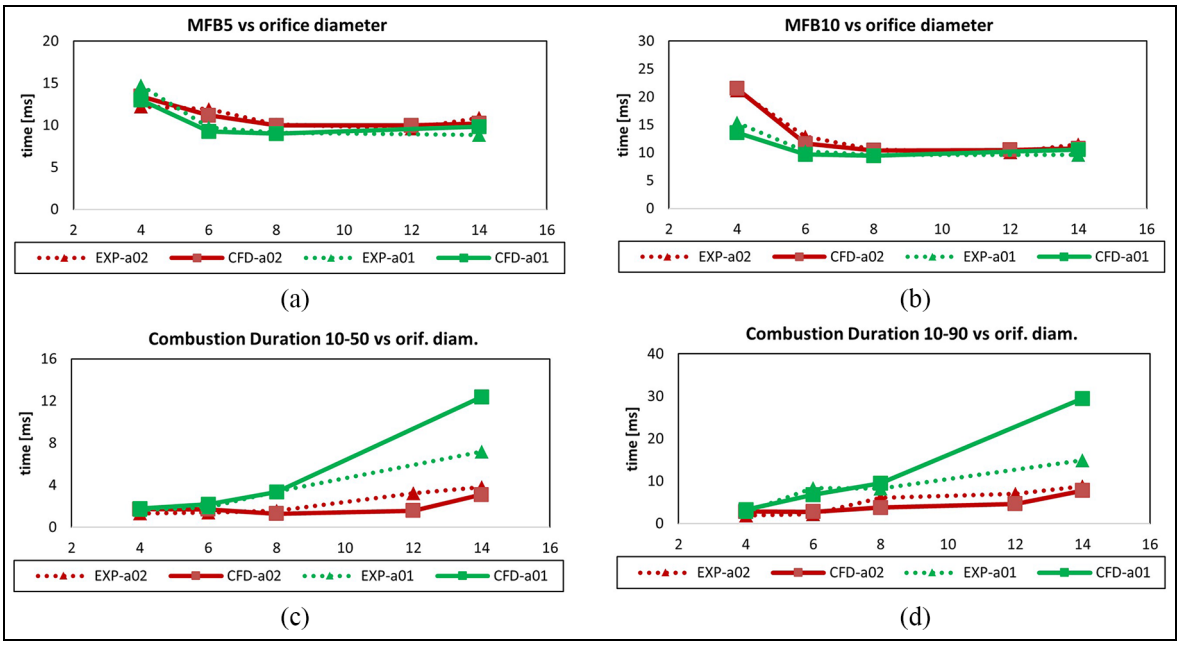

Figure 27. Ignition delay and combustion orifice varying the orifice diameter, $a = 10\%$.

dynamically switching between chemistry- and turbulence-limited reaction rate would result in improved investigation capabilities.

Declaration of conflicting interests

The author(s) declared no potential conflicts of interest with respect to the research, authorship, and/or publication of this article.

Funding

The author(s) received no financial support for the research, authorship, and/or publication of this article.

ORCID iDs

Mattia Olcuire https://orcid.org/0000-0003-1940-8180
Clara Iacovano https://orcid.org/0000-0002-1331-0492
Tommaso Lucchini https://orcid.org/0000-0001-7677-8087
Stefano Fontanesi https://orcid.org/0000-0002-3303-4229

References

1. Yong JY, Ramachandaramurthy VK, Tan KM, et al. A review on the state-of-the-art technologies of electric vehicle, its impacts and prospects. *Renew Sustain Energ Rev* 2015; 49: 365–385.
2. Mangeruga V, Giacopini M, Barbieri SG, et al. Design of a hybrid power unit for formula SAE application:

packaging optimization and thermomechanical design of the electric motor case. *SAE paper 2019-24-0197*, 2019.
3. Hageman MD, Sakai SS and Rothamer DA. Determination of soot onset and background particulate levels in a spark-ignition engine. *Proc Combust Inst* 2015; 35: 2949–2956.
4. Cho ES and Chung SH. Improvement of flame stability and NOx reduction in hydrogen-added ultra lean premixed combustion. *J Mech Sci Technol* 2009; 23(3): 650–658.
5. D'Adamo A, Breda S, Fontanesi S, et al. A RANS knock model to predict the statistical occurrence of engine knock. *Appl Energy* 2017; 191: 251–263.
6. D'Adamo A, Breda S, Fontanesi S, et al. A RANS-based CFD model to predict the statistical occurrence of knock in spark-ignition engines. *SAE Int J Engines* 2016; 9(1): 618–630.
7. Breda S, D'Adamo A, Fontanesi S, et al. CFD analysis of combustion and knock in an optically accessible GDI engine. *SAE Int J Engines* 2016; 9: 641–656.
8. Quader AA. Lean combustion and the misfire limit in spark ignition engines. *SAE paper 741055*, 1974.
9. Germane GJ, Wood CG and Hess CC. Lean combustion in spark-ignited internal combustion engines: a review. *SAE paper 831694*, 1983.
10. D'Adamo A, Breda S, Berni F, et al. Understanding the origin of cycle-to-cycle variation using large-eddy simulation: similarities and differences between a homogeneous low-revving speed research engine and a production DI turbocharged engine. *SAE Int J Engines* 2018; 12(1): 45–56.
11. Chinnathambi P, Thelen B, Cook D, et al. Performance metrics for fueled and unfueled turbulent jet igniters in a rapid compression machine. *Appl Therm Eng* 2021; 182: 115893.
12. Benekos S, Frouzakis CE, Giannakopoulos GK, et al. Prechamber ignition: an exploratory 2-D DNS study of the effects of initial temperature and main chamber composition. *Combust Flame* 2020; 215: 10–27.
13. Distaso E, Amirante R, Cassone E, et al. Experimental and numerical analysis of a pre-chamber turbulent jet ignition combustion system. *SAE paper 2019-24-0018*, 2019.
14. Attard WP, Fraser N, Parsons P, et al. A turbulent jet ignition pre-chamber combustion system for large fuel economy improvements in a modern vehicle powertrain. *SAE Int J Engines* 2010; 3(2): 20–37.
15. Attard W, Kohn J and Parsons P. Ignition energy development for a spark initiated combustion system capable of high load, high efficiency and near zero NOx emissions. *SAE paper 20109088*, 2010.
16. Attard WP and Blaxill H. A gasoline fueled pre-chamber jet ignition combustion system at unthrottled conditions. *SAE Int J Engines* 2012; 5(2): 315–329.
17. Attard W and Blaxill H. A lean burn gasoline fueled prechamber jet ignition combustion system achieving high efficiency and low NOx at part load. *SAE paper 2012-01-1146*, 2012.
18. Tsuboi S, Miyokawa S, Matsuda M, et al. Influence of spark discharge characteristics on ignition and combustion process and the lean operation limit in a spark ignition engine. *Appl Energy* 2019; 250: 617–632.
19. Kyrtatos P, Bardis K, Bolla M, et al. Transferability of insights from fundamental investigations into practical applications of prechamber combustion systems. In: *4th IAV international conference on ignition systems for gasoline engines*, Berlin, Germany, 6–7 December 2018, pp.442–459. Berlin: IAV.
20. Bunce M, Blaxill H, Kulatilaka W, et al. The effects of turbulent jet characteristics on engine performance using a pre-chamber combustor. *SAE paper 2014-01-1195*, 2014.
21. Gentz G, Thelen B, Gholamisheeri M, et al. A study of the influence of orifice diameter on a turbulent jet ignition system through combustion visualization and performance characterization in a rapid compression machine. *Appl Therm Eng* 2015; 81: 399–411.
22. Biswas S, Tanvir S, Wang H, et al. On ignition mechanisms of premixed CH_4/air and H_2/air using a hot turbulent jet generated by pre-chamber combustion. *Appl Therm Eng* 2016; 106: 925–937.
23. Muller M, Freeman C, Zhao P, et al. Numerical simulation of ignition mechanism in the main chamber of turbulent jet ignition system. In: *Proceedings of the ASME 2018 internal combustion engine division fall technical conference. Volume 2: emissions control systems; instrumentation, controls, and hybrids; numerical simulation; engine design and mechanical development*, San Diego, CA, 4–7 November 2018. New York: ASME.
24. Bunce M and Blaxill H. Methodology for combustion analysis of a Spark ignition engine incorporating a prechamber combustor. *SAE paper 2014-01-2603*, 2014.
25. Malé Q, Staffelbach G, Vermorel O, et al. Large eddy simulation of pre-chamber ignition in an internal combustion engine. *Flow Turbul Combust* 2019; 103: 465–483.
26. Gholamisheeri M, Wichman IS and Toulson E. A study of the turbulent jet flow field in a methane fueled turbulent jet ignition (TJI) system. *Combust Flame* 2017; 183: 194–206.
27. Gholamisheeri M, Thelen BC, Gentz GR, et al. Rapid compression machine study of a premixed, variable inlet density and flow rate, confined turbulent jet. *Combust Flame* 2016; 169: 321–332.
28. Bolla M, Shapiro E, Tiney N, et al. Numerical simulations of pre-chamber combustion in an optically accessible RCEM. *SAE paper 2019-01-0224*, 2019.
29. Shapiro E, Tiney N, Kyrtatos P, et al. Experimental and numerical analysis of pre-chamber combustion systems for lean burn gas engines. *SAE paper 2019-01-0260*, 2019.
30. Xu G, Kotzagianni M, Kyrtatos P, et al. Experimental and numerical investigations of the unscavenged prechamber combustion in a rapid compression and expansion machine under engine-like conditions. *Combust Flame* 2019; 204: 68–84.
31. Yamaguchi S, Ohiwa N and Hasegawa T. Ignition and burning process in a divided chamber bomb. *Combust Flame* 1985; 59: 177–187.
32. Berni F, Cicalese G and Fontanesi S. A modified thermal wall function for the estimation of gas-to-wall heat fluxes in CFD in-cylinder simulations of high performance spark-ignition engines. *Appl Therm Eng* 2017; 115: 1045–1062.
33. Berni F and Fontanesi S. A 3D-CFD methodology to investigate boundary layers and assess the applicability

of wall functions in actual industrial problems: a focus on in-cylinder simulations. *Appl Therm Eng* 2020; 174: 115320.
34. Berni F, Cicalese G, Sparacino S, et al. On the existence of universal wall functions in in-cylinder simulations using a low-Reynolds RANS turbulence model. *AIP Conf Proc* 2019; 2191: 020019.
35. Qin Z, Lissianski VV, Yang H, et al. Combustion chemistry of propane: a case study of detailed reaction mechanism optimization. *Proc Combust Inst* 2000; 28: 1663–1669.
36. Blint RJ. The relationship of the laminar flame width to flame speed. *Combust Sci Technol* 1986; 49(1–2): 79–92.
37. Vancoillie J, Demuynck J, Galle J, et al. A laminar burning velocity and flame thickness correlation for ethanol-air mixtures valid at spark-ignition engine conditions. *Fuel* 2012; 102: 460–469.
38. D'Adamo A, Del Pecchia M, Breda S, et al. Chemistry-based laminar flame speed correlations for a wide range of engine conditions for iso-octane, n-heptane, toluene and gasoline surrogate fuels. *SAE paper 2017-01-2190*, 2017.
39. Del Pecchia M, Breda S, D'Adamo A, et al. Development of chemistry-based laminar flame speed correlation for part-load SI conditions and validation in a GDI research engine. *SAE Int J Engines* 2018; 11(6): 715–741.
40. Del Pecchia M, Pessina V, Berni F, et al. Gasoline-ethanol blend formulation to mimic laminar flame speed and auto-ignition quality in automotive engines. *Fuel* 2020; 264: 116741.
41. D'Adamo A, Iacovano C and Fontanesi S. Large-Eddy simulation of lean and ultra-lean combustion using advanced ignition modelling in a transparent combustion chamber engine. *Appl Energy* 2020; 280: 115949.
42. Peters N. *Turbulent combustion*. 1st ed. Cambridge: Cambridge University Press, 2000.
43. Peters N. Laminar Flamelet Concepts in Turbulent Combustion. In: *Twenty first international symposium on combustion*, Technical University of Munich, Germany, 3–8 August 1986, pp.1231–1250. Pittsburgh: The Combustion Institute.
44. Abdel-Gayed RG, Bradley D and Lung FKK. Combustion regimes and the straining of turbulent premixed flames. *Combust Flame* 1989; 76(2): 213–218.
45. Poinsot T, Veynante D and Candel S. Diagrams of premixed turbulent combustion based on direct simulation. In: *Twenty-third international symposium on combustion*, University of Orléans, France, 22–27 July 1990, pp.613–619. Pittsburgh: The Combustion Institute.
46. Iacovano C, D'Adamo A and Cantore G. Analysis and simulation of non-flamelet turbulent combustion in a research optical engine. *Energy Proc* 2018; 148: 463–470.

Appendix

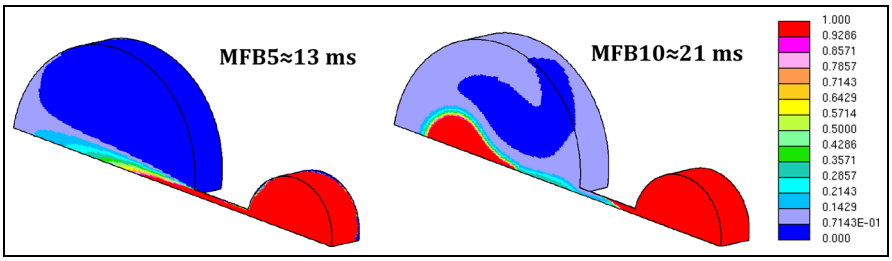

Figure A1. Progress variable at MFB5 and MFB10, respectively to 13 and 21 ms, coincident with the pressure changes in slope, $a = 20\%$, $D = 4$ mm.

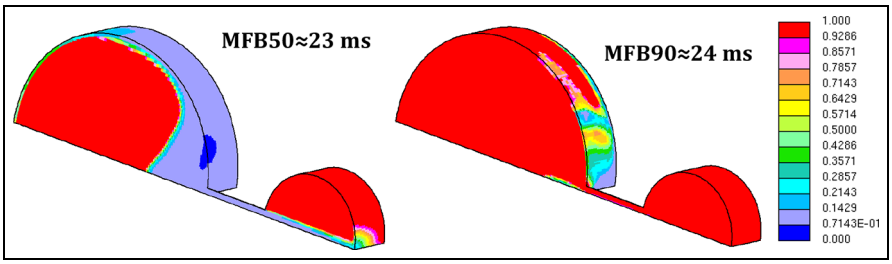

Figure A2. Progress variable at MFB50 and MFB90, respectively to 23 and 24 ms, $a = 20\%$, $d = 4$ mm.

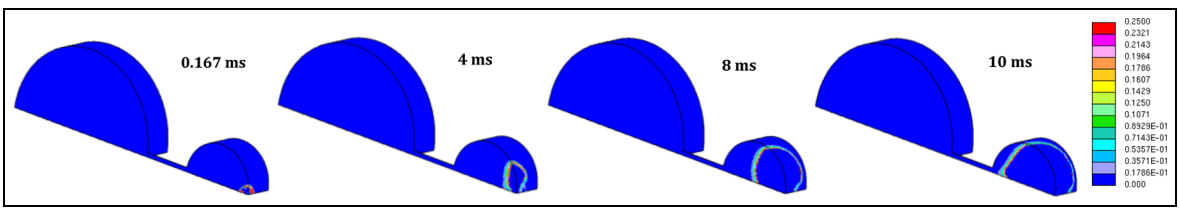

Figure A3. Pre-chamber chemical reaction front, $a = 0.2$ and $d = 4$ mm case.

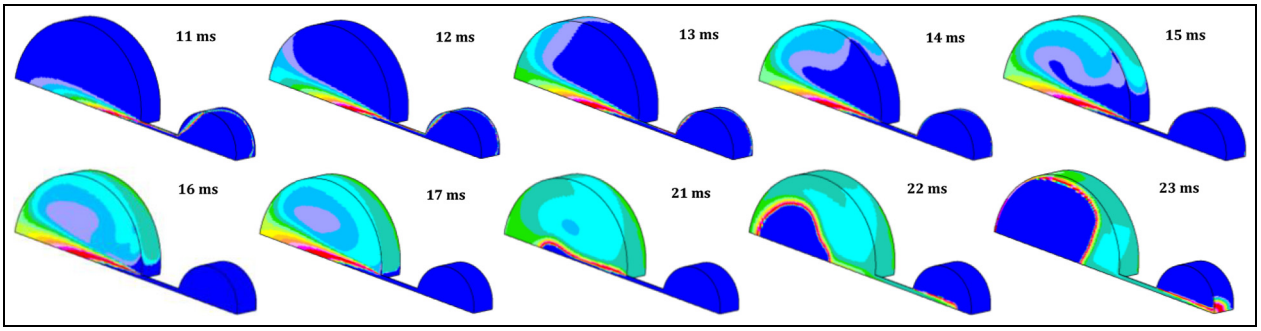

Figure A4. Main chamber chemical reaction front, $a = 20\%$ and $d = 4$ mm case. Once the chocking phase occurs, the chemical species spread into the main chamber, strongly increasing the reaction zone area and facilitating the subsequent flame ignition.